communications earth & environment

ARTICLE

https://doi.org/10.1038/s43247-023-01193-7 OPEN

The foundations of the Patagonian icefields

Johannes J. Fürst[1✉], David Farías-Barahona[1,2], Norbert Blindow[1], Gino Casassa[3,4], Guisella Gacitúa[5], Michèle Koppes[6], Emanuele Lodolo[7], Romain Millan[8,9], Masahiro Minowa[10], Jérémie Mouginot[9], Michał Pętlicki[11,12], Eric Rignot[13,14], Andres Rivera[15], Pedro Skvarca[16], Martin Stuefer[17], Shin Sugiyama[10], José Uribe[11], Rodrigo Zamora[11], Matthias H. Braun[1], Fabien Gillet-Chaulet[9], Philipp Malz[1], Wolfgang J.-H. Meier[1] & Marius Schaefer[18]

The two vast Patagonian icefields are a global hotspot for ice-loss. However, not much is known about the total ice volume they store - let alone its spatial distribution. One reason is that the abundant record of direct thickness measurements has never been systematically exploited. Here, this record is combined with remotely-sensed information on past ice thickness mapped from glacier retreat. Both datasets are incorporated in a state-of-the-art, mass-conservation approach to produce a well-informed map of the basal topography beneath the icefields. Its major asset is the reliability increase of thicknesses values along the many marine- and lake-terminating glaciers. For these, frontal ice-discharge is notably lower than previously reported. This finding implies that direct climatic control was more influential for past ice loss. We redact a total volume for both icefields in 2000 of 5351 km^3. Despite the wealth of observations used in this assessment, relative volume uncertainties remain elevated.

[1] Institute of Geography, Friedrich-Alexander Universität Erlangen-Nürnberg, Erlangen, Germany. [2] Departamento de Geografía, Universidad de Concepción, Concepción, Chile. [3] Centro de Investigación Gaia Antártica, Universidad de Magallanes, Punta Arenas, Chile. [4] Unidad de Glaciología y Nieves, Dirección General de Aguas, Ministerio de Obras Públicas, Santiago de Chile, Chile. [5] National Center for Climate Research, Danish Meteorological Institute, Copenhagen, Denmark. [6] Department of Geography, Faculty of Arts, The University of British Columbia, Vancouver, BC, Canada. [7] Istituto Nazionale di Oceanografia e di Geofisica Sperimentale, Trieste, Italy. [8] Department of Geosciences and Natural Resources Management, University of Copenhagen, Copenhagen, Denmark. [9] Université Grenoble Alpes, CNRS, INRAE, IRD, Grenoble INP, IGE, Grenoble, France. [10] Institute of Low Temperature Science, Hokkaido University, Sapporo, Japan. [11] Centro de Estudios Científicos, Valdivia, Chile. [12] Faculty of Geography and Geology, Jagiellonian University, Kraków, Poland. [13] Department of Earth System Science, University of California, Irvine, CA, USA. [14] Radar Science and Engineering, NASA's Jet Propulsion Laboratory, Pasadena, CA, USA. [15] Departamento de Geografía, Universidad de Chile, Región Metropolitana, Chile. [16] Glaciarium - Glacier Interpretive Center, El Calafate, Argentina. [17] Geophysical Institute, University of Alaska Fairbanks, Fairbanks, AK, USA. [18] Instituto de Ciencias Físicas y Matemáticas, Universidad Austral de Chile, Valdivia, Chile. ✉email: johannes.fuerst@fau.de

Disregarding glaciers and ice caps at the ice-sheet peripheries, the Southern Hemisphere accommodates about 6% of the global glacier-ice volume[1,2]. This fraction has the potential to raise global mean sea-level by about 15 mm. It is remarkable that 80% of this volume is stored in only two ice bodies in the Southern Andes - the Patagonian icefields (PIs). The Southern Patagonian Icefield (SPI) is about three times larger than the Northern Patagonian Icefield (NPI). In 2000, the combined ice masses of the PIs covered a surface comparable to the metropolitan area of Paris (~16,000 km^2)[3,4], and showed average thickness values that exceed 250 m. This implies that PI glaciers are typically five times thicker than their European counterparts. In total, they store forty times more ice volume than glaciers in the European Alps. The Patagonian climate is characterised by westerly winds impinging on the Andean Cordillera resulting in a unique atmospheric gradient from super-humid conditions in the west to arid conditions in the east[5]. Prolific moisture transport results in inimitable amounts of annual precipitation[6–10]. High mass turn-over of glacier ice is the consequence, with maximum flow speeds reaching several kilometres a year[11]. Such velocity magnitudes are comparable to the largest outlet glaciers in Greenland and Antarctica[12–15]. Moreover, gravimetry measurements indicate that the vast ice plateau of the interior shows thickness values that exceed 1000 m[16]. Again, this is exceptional for glacierised regions outside the large ice sheets.

In the recent past, we have observed widespread thinning over the PIs. Specific ice-loss rates not only exceed values observed in nearby regions[17,18] but are also elevated as compared to other mountain ranges around the globe[19,20]. The primary reason for this exceptional mass loss is controversial. The dominant driver is either direct climatic forcing or ice-dynamics. The former relates to mass gain and loss at the glacier surface, i.e. the surface mass balance (SMB). Ice-dynamic losses exclusively occur at marine- and lake-terminating (MALT) ice fronts. The ice-dynamic losses are typically subsumed under frontal ablation, which comprises iceberg calving and subaqueous melting. A final judgement of the dominant mass-loss term remains evasive because of the poorly constrained SMB processes[6,8] as well as the little knowledge of ice thickness near the glacier snouts[21]. The reasons for this are the strong climate gradients in the region, the temperate nature of glacier ice as well as the general inaccessibility of the MALT glacier trunks (remoteness, crevassing, etc.).

Many attempts have been made to estimate how much ice is stored in the PIs and how it is distributed. Recent studies with a global focus[1,2] relied on principles of mass conservation, the shallow ice approximation or a combination of the two. These studies were calibrated with measurements in the Glacier Thickness Database (GlaThiDa)[22,23]. Up to its latest version, GlaThiDa3.1.0, no direct measurements were included for either icefield in Patagonia. Therefore, the quality of these thickness maps ultimately depends on the transferability of these approaches between regions. Thickness reconstructions with a regional focus on South America[16,24,25] are based on the yield-stress assumption or on gravimetric inversions. These studies attempted to constrain the thickness map with available measurements. Often this meant using selected survey campaigns on the low-elevation trunks of just a few glaciers. For gravimetric inversions[16,25], abundant measurement records were available over the plateau areas. However, coverage of the elongated glacier trunks is poor. In summary, available thickness maps are largely unconstrained and often ignore the region-specific climatic, ice-dynamic and geometric setting. Moreover, thickness maps are particularly unreliable along the low-elevation outlet-glacier trunks.

Apart from the mere interest in the ice volume or its spatial distribution, glaciers are key elements with socio-economic and ecological importance[26–30]. In terms of natural resource, they act as natural water reservoirs. In this role, questions arise such as when peak water is reached under future warming[27] and to what extent glaciers continue to buffer fresh-water shortage during dry seasons[31]. Such questions rely on future glacier projections. Their reliability is ultimately tied to the knowledge of present-day ice thickness[32,33]. As glaciers retreated in recent decades, new proglacial lakes formed while others expanded[34]. Although such lakes are potential sites for future hydro-power generation[29], they also pose a threat to downstream communities, if dams break. In a review of glacier related hazards for Chile and Argentina[35], the authors appeal for a research intensification in mountainous regions on the influence of cryospheric changes on slope failures and on outburst floods. The basis for such research is solid knowledge on the basal topography beneath the ice cover. Finally and on global scales, there is evidence that glacier retreat impacts positively on biodiversity[28]. This idealistic picture is moderated by the fact that particular species, adapted to glacial conditions, are often losers under these changes. In Tierra del Fuego, phytoplankton biomass reduction was observed in fjord systems as glacier retreated[36]. For further details, we refer the interested reader to a recent overview of the environmental impacts of glacier changes in Chile[37]. In summary, glacier thickness mapping is relevant far beyond the mere interest in sea-level relevant melt volume.

The primary objective of this study is to compile available thickness surveys, many of which were not considered previously. In addition, multi-temporal remote sensing of glacier elevation and outline changes is used to infer past thickness values in areas that have become ice free. This glacier retreat information represents additional near-front data. All thickness observations are assimilated with a state-of-the-art reconstruction approach for mapping glacier ice thickness that combines two methods. One method makes use of the principles of mass conservation[38,39] and converts ice flux to thickness values using the shallow-ice approximation (SIA)[40]. The other method relies on the perfect plasticity assumption (PPA) for describing the ice rheology (for details see Data & Methods). Thickness results from both methods are updated in regions of fast ice flow according to velocity observations and subsequently combined into a multi-model reconstruction. The chosen reconstruction approach will thereby account for model-based SMB estimates, reflecting the climatic state, as well as remotely sensed information on the geometric setting, recent elevation changes and the ice-dynamic conditions. Apart from targeting a multi-model thickness map for both icefields, a primary motivation is to better constrain the dominant drivers for recent mass loss.

Results and discussion

The multi-model reconstruction approach provides a distributed field of ice thickness, together with associated uncertainties and the underlying bedrock topography (Fig. 1). The thickness map has a timestamp of 2000 stemming from the reference geometric state as defined by the digital elevation model (DEM) from the Shuttle Radar Topography Mission (SRTM)[41]. Contemporaneous glacier outlines are taken from the Randolph Glacier Inventory version 6.0 (RGI6.0)[3,4]. The maps are presented on a 200-m resolution. Direct and indirect thickness information is imprinted (cf. Data and Methods, Supplementary Fig. S5).

Ice volume. By integrating the ice-thickness maps, ice volumes of 1156 ± 398 and 4195 ± 1362 km^3 are computed for NPI and SPI (Table 1), respectively. On the one hand, the NPI volume is at the lower end of previous estimates but agrees within ~10% considering temporal differences. On the other hand, the SPI volume

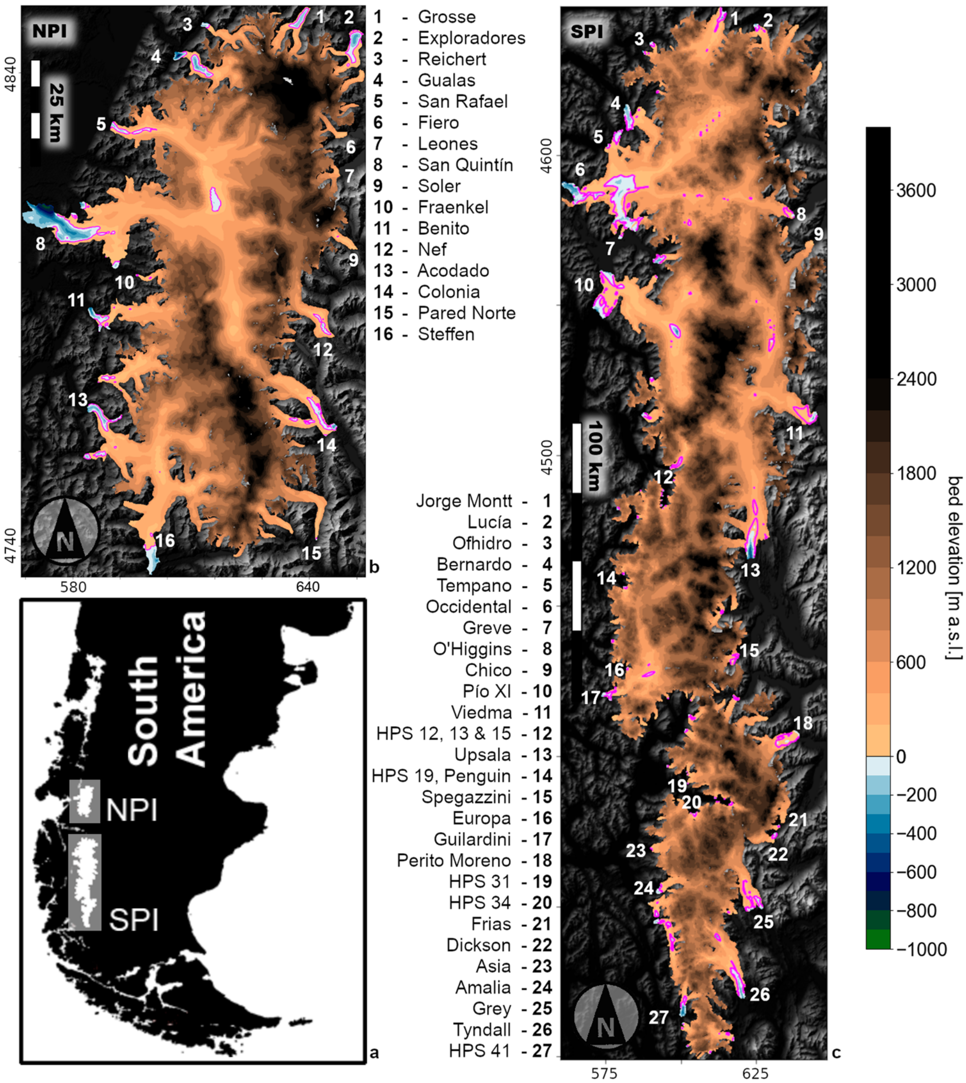

Fig. 1 The ice-free topography beneath the Patagonian icefields. a Overview panel for icefield locations. **b** NPI basal topography. **c** SPI basal topography in metres above sea level (ma.s.l.). The magenta lines delineate areas below sea- or lake level per adjacent glacier drainage basin. Coordinates: UTM 18S in kilometres. Background: SRTM hillshade.

is at the upper end and the disagreement to previous estimates increases to 25%. Ignoring the low-biased consensus estimate[1], the agreement values reduce again to the same level as for NPI.

Concerning the associated volume uncertainties, we find relative values above 30% for both icefields (Table 1). All previous volume estimates fall into these ranges. Most previous studies were more optimistic about their uncertainty assessments. We are surprised that our approach produces higher errors, compared to these other studies, because a substantially larger amount of thickness measurements were considered. When averaging the relative measurement error of the thickness observations themselves (cf. Data & Methods), we obtain a mean value of 28% (standard deviation 16%). Admittedly, this average can only serve as a loose orientation and the final volume error will depend on the specific spatial distribution of these measurements. However, we assume that it is unlikely that a much lower relative volume error can be achieved, and values below 20% do not seem justifiable for the PIs.

Frontal areas & outlet glaciers. Knowing the thickness distribution and the basal topography, we can infer the volume fraction of glacier ice that lies below flotation (BF), i.e. not contributing to sea-level when melted. For both icefields only a small fraction (1–2%) is situated below flotation (Table 1). This ice is located in a confined area of 189 km^2 on NPI and 445 km^2 on SPI, representing about 4–5% of the total icefield extent. Considering the current areal retreat rates of 0.2–0.5% yr^{-1} for NPI and 0.2% yr^{-1} for SPI, this area is imminently at risk. This is certainly the case for SPI, where half of the mass loss occurs as frontal ablation at the ice fronts of MALT glaciers[21]. Except for the low-biased consensus estimate[1], previous thickness maps often suggest more than twice as much BF ice. The moderate BF-volume reported here is somewhat in contrast to our high-end estimate of the total SPI volume. This contrast is a first indication that outlet glaciers tend to be thinner than previously thought.

The new PI bedrock maps show many glaciers with deeply incised troughs that lie below sea- or lake-level (Fig. 1). With respect to depth and areal extent, the most prominent incisions are found for Glaciar San Quintín in NPI and Glaciar Upsala in SPI. For the former glacier, the bed over-deepening reaches almost 20-km inland - a potentially susceptible setup for future retreat. This susceptibility assessment is based on paleo-evidence from an Arctic outlet glacier[42] as well as centennial glacier retreat in Patagonia and Tierra del Fuego[43–48]. Episodes of fast retreat of

Table 1 Icefield volume estimates

	Carrivick et al. (2016)[24]	Millan et al. (2019)[25]	Farinotti et al. (2019)[1]	Millan et al. (2022)[2]	this study
Original time stamp	2009	2015	2000	2017–2018	2000
Reference time stamp	**2000**	**2000**	**2000**	**2000**	**2000**
NPI	1235 ± 247[a]	1124 ± 260[a]	1069 ± 277[b,d,e]	1203 ± 326[b,d,f]	1156 ± 398[c]
below flotation	*54 (247)*[b]	*30 (189)*[b]	*16 (103)*[b]	*51 (228)*[b]	*29 (189)*[b]
	1277 ± 255	**1194 ± 276**	**1069 ± 277**	**1284 ± 348**	**1156 ± 398[c]**
SPI	4327 ± 865[a]	3632 ± 675[a]	3332 ± 865[b,d]	3915 ± 1062[b,d]	4195 ± 1362[c]
below flotation	*284 (1201)*[b,g]	*219 (1001)*[b,g]	*32 (325)*[b]	*134 (800)*[b,g]	*57 (445)*[b]
	4447 ± 889	**3832 ± 712**	**3332 ± 865**	**4149 ± 1125**	**4195 ± 1362[c]**

Values are given in cubic kilometres (km^3) ice equivalent (i.e.). The volume fraction below flotation (italic numbers) does not contribute to sea-level rise, if lost. The respective areal extent of the ice below flotation (in italic and in parenthesis) is provided in square kilometres (km^2). Furthermore, volume estimates are homogenised to the year 2000 (bold numbers) using geodetic loss rates of − 4.65 $km^3\ yr^{-1}$ for NPI and − 13.35 $km^3\ yr^{-1}$ for SPI[17]. These rates are linearly scaled with the elapsed time. Respective uncertainties in 2000 are scaled with the total volume.
Bold numbers refer to the year 2000.
Italic numbers refer to volume fraction below flotation (km^3) and the respective areal extent (km^2) is given in parenthesis.
[a]Volume value and uncertainty directly taken from respective article.
[b]Volume (and area) computed from available maps. For lake-terminating glaciers, lake levels have been considered for lakes larger than 20 km^2.
[c]For computing volume errors, associated error maps are capped to 50% of the local ice thickness.
[d]Relative uncertainty estimated from Southern Andes volume uncertainty of 27% for Millan et al. (2022)[2] or from global volume uncertainty 26% for Farinotti et al. (2019)[1].
[e]Thickness information is missing for central parts of NPI (~50 km^2).
[f]Thickness information is missing in high elevated areas of Glaciar Steffen.
[g]DEM information approximated with SRTM or TDX2019.

MALT glaciers preferentially occurred along over-deepened bed sections. Further over-deepened sections beneath the NPI are found for Grosse and Exploradores glaciers in the north and Glaciar Nef in the east. At Glaciar Upsala in the SPI, frontal bathymetry locally exceeds 700 m below present lake level (179 m a.s.l.). However, the bed topography is prograde, certainly from its current front, that is to say it increases upglacier. This implies a more stable setup under retreat. Prograde bed topographies seem more characteristic for glacier fronts of SPI. A prominent exception is Glaciar Perito Moreno, for which the bedrock topography reaches up to 300 m below the lake level some 4 km from the ice-front. Near the ice-front, values range between 30 and 140 m, which is small compared to direct bathymetric measurements of up to 160 m in the adjacent lakes themselves[49,50]. Further north, the marine-terminating Glaciar Pío XI - the largest glacier in SPI - drains more than 10% of the ice field area into Eyre Fjord. Its trunk thickness is unsurveyed. Our approach suggests that the bathymetry is rather shallow near the front (<100 m) and in vast areas the bed remains above sea-level. This is in accordance with aerial images from the 1940s (Fig. 2), which show a much receded glacier front compared to its present-day position. An exposed outwash plain is visible in the area currently covered by the northern glacier branch and an ice-dammed proglacial lake. For further discussion of selected glacier examples, we point the interested reader to Supplementary Section S3. The identification of over-deepened bed sections can only be the first step to point out susceptible glacier setups. Yet, the pre-conditioning, the onset and the duration of phases of fast retreat is complex as they not only depend on the exact bedrock details. These phases are additionally controlled by the general ice-flow regime[32], the thermal and circulation conditions in the pro-glacial water body[21,51–53], the climatic or SMB history[54,55] as well as glacier response times[56].

Thickness distribution and aggregated performance. Here, the analysis will focus on the thickness distribution and its comparison to independent observations and other map estimates (Fig. 3). In the interior, our reconstructed thickness field agrees well with the gravimetry inversion[25] (Fig. 3c). The reason is that values of the latter inverted map were used as an input to this study along the actual flight-lines of the underlying gravity survey (Supplementary Fig. S5). Two more recent map estimates (Fig. 3d, e and Supplementary Fig. S1d, e), based on a global multi-model consensus or velocity observations, appear somewhat shallower in the interior. Close to ice-free areas and nunataks, thickness values increase much quicker with distance as compared to some of the previous maps (Fig. 3a, d, e). The resultant steeper mountain flanks are more consistent with the surrounding ice-free high-relief topography. This has important consequences for slope stability assessments[26]. Further discussion on the valley shape is presented in Supplementary Section S3.

The participant approaches in the consensus estimate[1] often pursue the reconstruction along flow lines or elevation bands and the final map interpolation depends on local slopes[1,57,58]. This dependence introduces a patchy pattern in the ice thickness distribution. On NPI, San Rafael and San Quintín glaciers are prime examples (Fig. 3d). Also the velocity-based approach (Fig. 3e) shows this erratic pattern because it relies on the SIA, which is equally sensitive to surface slope. Our estimate is less affected (Fig. 3a). The reason is that for the fast-flowing glacier units, it exclusively builds on mass conservation and is thereby independent of local slope magnitudes.

We aggregate the differences between modelled and observed values of ice thickness from each measurement location into scalar metrics (Fig. 4, Supplementary Fig. S4). These metrics serve as an overall evaluation for the various thickness maps. On NPI, mean and median differences are considerably smaller than in previous studies. This is less clearly expressed for SPI. Standard deviations, as a measure of the scattering of these differences, are lower for our approach on both icefields. This primarily reflects our systematic assimilation of ground-truth data. More details on these metrics are discussed in Supplementary Section S3. In summary, we are convinced that our thickness maps show improved quality mainly along fast-flowing outlet glaciers, as these areas are ideally suited for our method and because direct thickness measurements are concentrated there (Supplementary Fig. S5b, d).

Frontal ice discharge. For the remainder of this section, we will focus on frontal ablation or more specifically on the frontal ice discharge (cf. Data & Methods). It is computed along flux gates (FG) using our thickness map, 2004 velocity information[11] and a down-glacier correction for apparent mass balance. For NPI, the total discharge of $1.61 \pm 0.29\ km^3\ yr^{-1}$ is ~40% smaller (Fig. 5) than inferred in a recent FG study[21]. Also for SPI, we find a value which is about 25% lower than the aforementioned study, i.e. $16.48 \pm 2.56\ km^3\ yr^{-1}$. Part of these differences are certainly

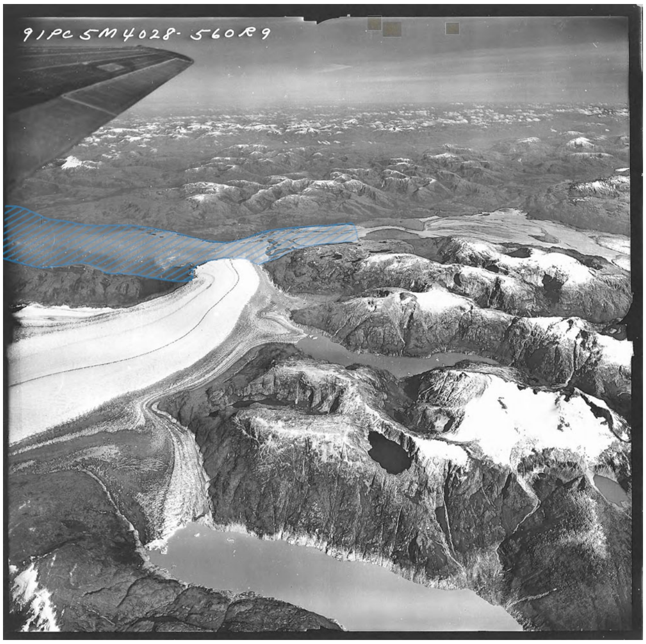

Fig. 2 Aerial photograph of Glaciar Pío XI. The photo was taken on February 15, 1945 at 10:48am by the US Air Force using a trimetrogon camera[74,75]. The glacier calves into Eyre Fjord (centre left). Towards the north (centre, right), a large outwash plane is seen in areas which are now covered by the glacier itself or Lago Greve. The blue hatching loosely follows the fjord outlines as well as the outwash plane that are now covered by Glaciar Pío XI. Photo courtesy: Geographical Military Institute (IGM) of Chile.

explained by glacier retreat, which is neglected in our study. However, the discrepancy mostly arises from just a few glaciers. For NPI, Glaciar San Quintín is found to export less than one third of the ice than previously thought. The remaining difference in total ice discharge stems from some other MALT glaciers being prolific (e.g., Acodado, Steffen, Nef, Leones). For Glaciar Nef, the low value is well constrained by extensive thickness surveys. In the case of Glaciar San Rafael, frontal thickness has been known for a long time and good agreement is seen between the various discharge estimates. Turning to SPI, a similar picture of reduced discharge arises. The prime example is Glaciar Pío XI, which we find to discharge about half as much ice, i.e. $1.48 \pm 0.21\,\mathrm{km^3 yr^{-1}}$. The main reason is that its front is significantly thinner than in previous estimates. Together with four other prominent glaciers, i.e. Penguin, Europa, HPS31 and O'Higgins, most of the reduction in the total discharge is explained. None of the discharge values of these glaciers are well constrained in terms of direct observations (Supplementary Fig. S5). More glacier examples are discussed in Supplementary Section S3. In summary, distinctly reduced frontal discharge values imply that climatically controlled surface processes must explain a larger share of the past ice loss.

Considering relative uncertainties in total ice discharge (Fig. 5), we find 18% and 16% for NPI and SPI, respectively. The previous study respectively reported 21% and 8%[21]. The lower relative uncertainty for SPI is surprising because much less is known about glaciers there, as compared to the NPI. An 8% discharge uncertainty appears, however, irreconcilable with typical errors of thickness measurements. Errors stemming from thickness mapping are the unequivocal and dominant source for uncertainties in frontal ablation (yellow whiskers in Fig. 5).

Independent estimates for frontal ablation are available from mass budgeting (MB) by differencing the integrated information on total geodetic mass change and SMB. The comparison with MB estimates of frontal ice discharge[6,8] reveals two aspects. First, mass budgeting suggests larger values for most outlet glaciers. The differences are important for SPI. Second, reported MB errors appear small as compared to the FG methods. Turning to icefield-wide scales, recent studies report an almost balanced SMB ($\pm 0.6\,\mathrm{km^3\,yr^{-1}}$) for NPI[6,9] (1975–2009) and +27.7 (1975–2000), $+40.1\,\mathrm{km^3\,yr^{-1}}$ (2000–2011) or $+29.9/31.5\,\mathrm{km^3\,yr^{-1}}$ (1975–2011) for SPI[8,9]. Another SMB study[7], which admits to not fully resolve melting along the narrow outlet glaciers, suggests even higher positive values of about +9 and $+55\,\mathrm{km^3\,yr^{-1}}$ (2000–2012) for NPI and SPI, respectively. Total mass-change values inferred by geodetic techniques using different satellite sensor systems agree well[17,18]. They amount to about -4.5 ± 0.2 and $-13.5 \pm 0.8\,\mathrm{km^3\,yr^{-1}}$ for NPI and SPI, respectively. The time period for the latter is about 2000 to 2012–2015. The residual between integrated values of the total mass change and the SMB (i.e., mass budgeting) gives information on ice loss across the lateral margin, i.e. frontal ablation. For both icefields, the differences are very large. The MB technique indicates a discharge value of over $40\,\mathrm{km^3\,yr^{-1}}$ for both NPI and SPI together. This value is twice as large than reported in this study. Neither the uncertainty associated to the geodetic method nor the conservative uncertainty estimates of our FG estimates allow a reconciliation with the SMB modelling efforts. Even the previous FG estimates for frontal ablation[21], which are somewhat larger, cannot close the mass budget. However, it is known that the SMB estimates suffer from the poorly quantified precipitation amounts over the Patagonian Andes[59]. Reasons are the sparse station network, which does not allow an adequate sampling and quantification of the singular zonal gradients in the atmopshere and of the extreme precipitation rates, especially at high elevation[5]. Moreover, existing SMB estimates remain to this day controversial and they likely suffer from overestimated precipitation amounts from regional climate models[10]. Precipitation amounts have been found to not be reconcilable with regional moisture availability in the atmosphere.

Let us turn to changes in the PI mass budget. Between 2000 and 2020, frontal ablation was virtually constant over the NPI[6] - a period in which total mass loss increased by $\sim 1.8\,\mathrm{km^3\,yr^{-1}}$[18]. For SPI, frontal ablation was reduced by about $\sim 4\,\mathrm{km^3\,yr^{-1}}$[21]. Yet mass loss rates only decreased by $\sim 2.0\,\mathrm{km^3\,yr^{-1}}$[18]. For both icefields, the discrepancy between changes in mass loss and frontal ablation requires a decreasing SMB. Again, the climatic influence seems to have had a more dominant control on past and recent ice loss from the PIs - and more so, than suggested in previous studies, considering the distinctly lower discharge estimates presented here.

Conclusions

This study is the first to compile and exploit available thickness surveys to estimate the ice-volume distribution of the two icefields in Patagonia in 2000. First, we suggest an upper-end ice volume estimate for Patagonia. The main reason is that the SPI likely stores 10% more ice than previously thought. Nonetheless, previous estimates remain within associated uncertainties. Despite making dedicated use of ground-truth data, this study cannot reduce and rather continues to produce large relative volume uncertainties exceeding 30%. These values ultimately stem from non-negligible errors inherent in the observations. The largest asset of this multi-model thickness map is that an abundant record of direct and indirect measurements is imprinted. In terms of thickness distribution, we are therefore convinced that the new basal topography represents an important quality increase, certainly along the many elongated outlet glaciers. Prominent examples are Glaciar San Quintín in NPI and Glaciar Upsala in

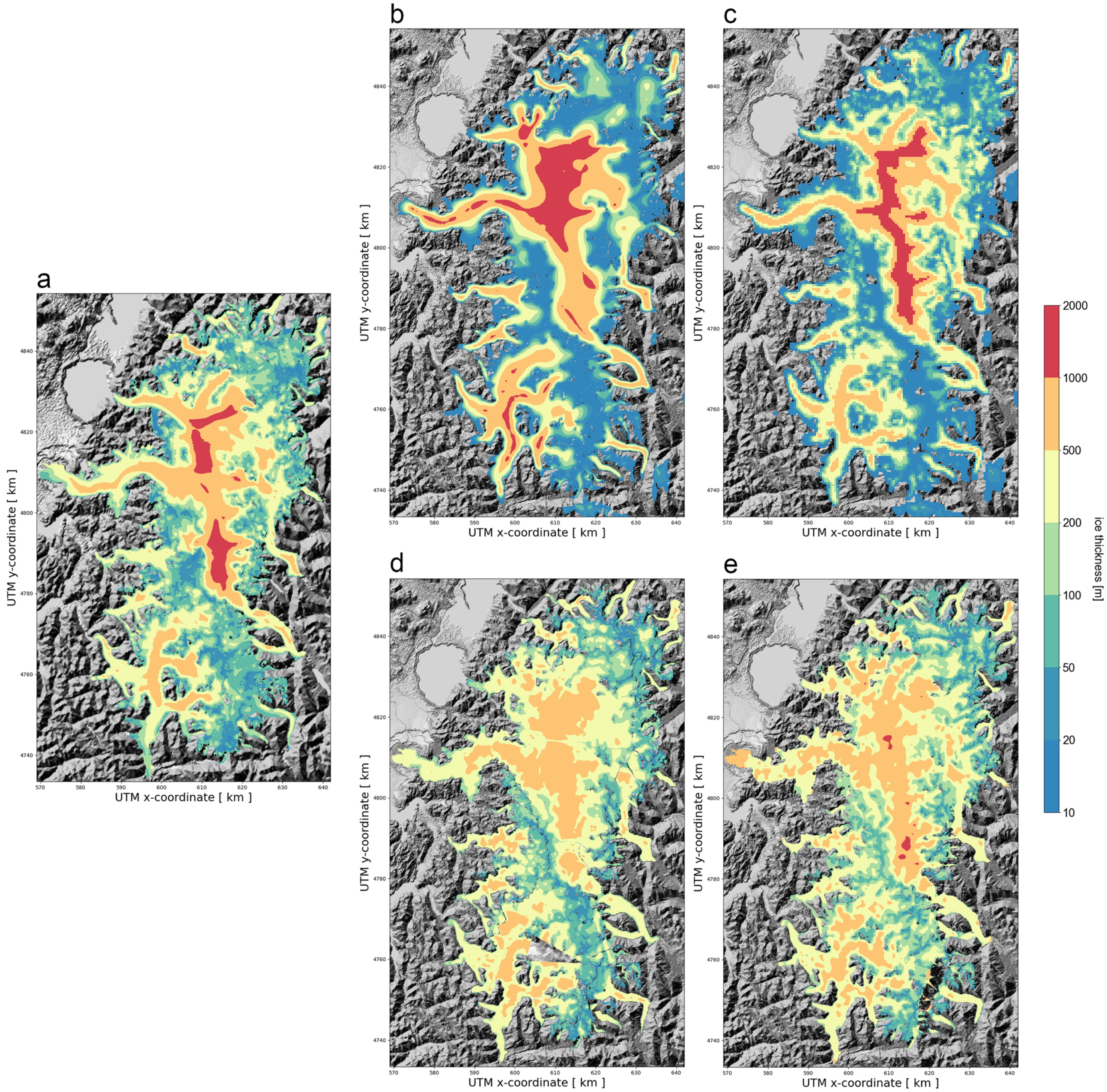

Fig. 3 NPI thickness distribution for various reconstructions. Distributions are shown for **a** this study and **b** the perfect plasticity estimate[24], **c** the gravimetry-based[25], **d** the global consensus[1] and **e** the global velocity-based estimates[2]. Background: SRTM hillshade.

SPI, two outlet glaciers, for which the trunk geometries are for the first time informed by direct measurements. We also find that our multi-model estimate appears beneficial in unsurveyed areas (e.g., Pío XI in Fig. 2). In summary, our basal topography map is key to reliably project future changes of the mountain cryosphere in Patagonia[32]. Such projections will present a solid basis to assess changes in regional fresh-water availability[27], hydrological turnover, biodiversity[28] and natural hazards[35]. Apart from the timing of future glacier retreat, the high quality of this map allows an improved identification of future lake formation - i.e., potential sites for hydro-power production[29].

Considering that the Patagonian icefields show elevated ice-loss rates in recent decades, it is a pressing task to partition the mass change into frontal ablation and surface mass balance. Assuming that the presented basal topography is more reliable along the MALT glaciers, frontal ice discharge estimates become more robust. For NPI and SPI, we find icefield-wide values of 1.6 and almost 16.5 km^3 yr^{-1}, respectively. For this 2000–2004 estimate we ignored glacier retreat. Previous discharge estimates diverge dependent on the underlying methodology. As compared to a recent study[21], ice-discharge values are lowered by more than 20%. This implies that surface processes, and with them the climatic influence, are likely more dominant drivers for mass loss from the Patagonian icefields, certainly when considering the discrepancy between recent changes in frontal ablation and total mass change[18,21].

In any case, there remains a very large discrepancy in frontal ablation with respect to residual estimates from mass budgeting, which involves integrated values of SMB and geodetic mass change. This discrepancy is actually an overestimation by mass budgeting, which is not covered by our conservative uncertainty estimate for frontal ablation. If we confide in the small

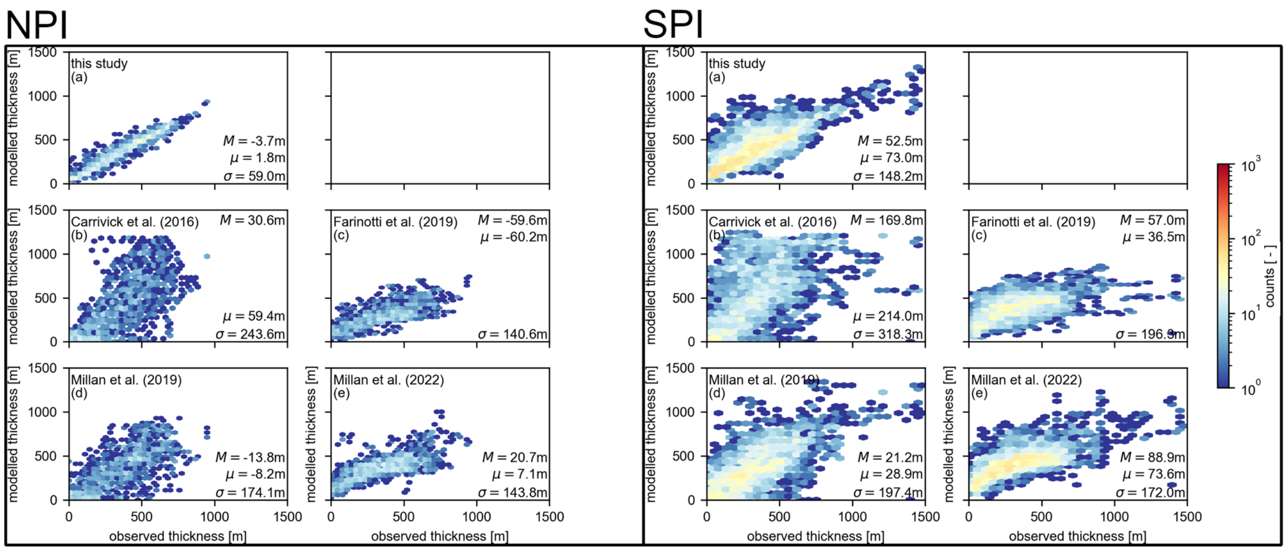

Fig. 4 Observed vs. reconstructed ice thickness. The comparison distinguishes between NPI and SPI. For the point-by-point comparison, respective thickness maps are bi-linearly interpolated to the measurement locations. For this figure, the measurement record only comprises borehole, seismic and GPR measurements. Thickness comparison is conducted for the map products from **a** this study, **b** the perfect-plasticity[24], **c** the global consensus[1], **d** the gravimetry-based[25] and **e** the global velocity-based estimates[2]. Values for mean (μ), median (M) and standard deviations (σ) are given.

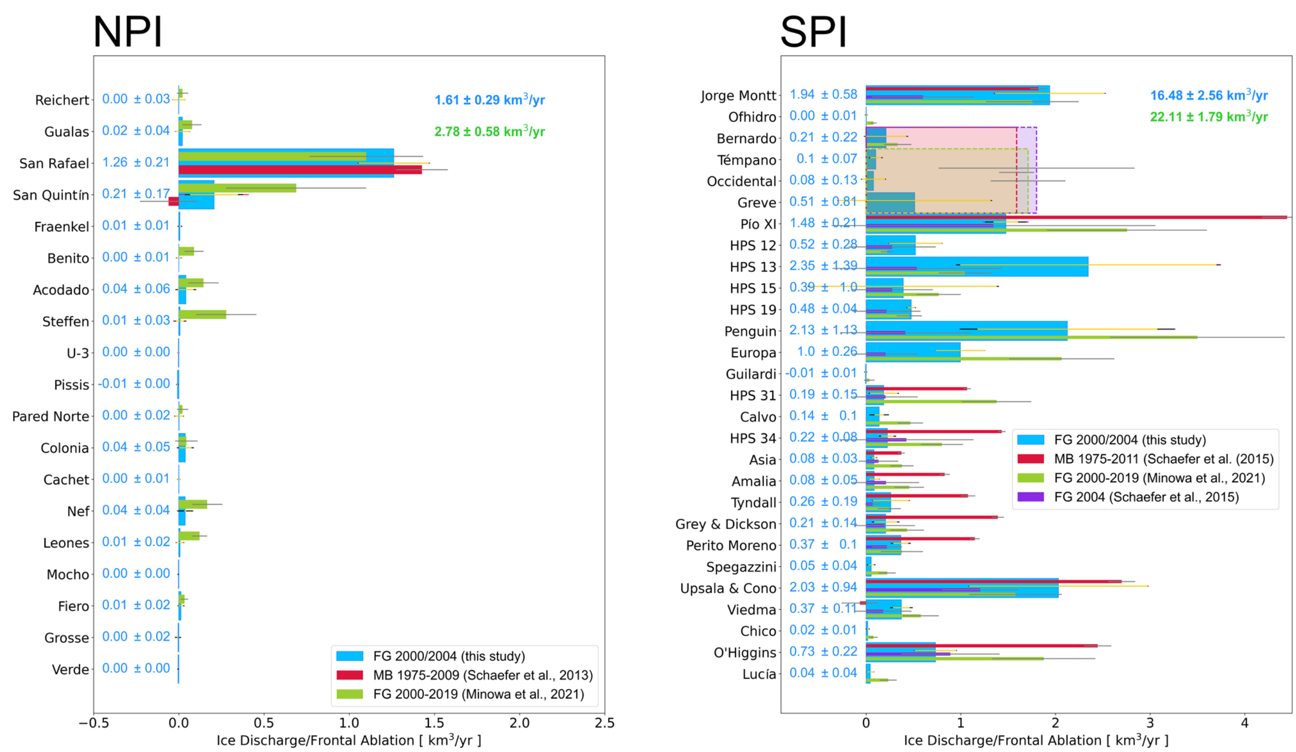

Fig. 5 Frontal Ice Discharge and Frontal Ablation. Values are given for the largest MALT glaciers in anticlockwise direction starting in the north of the icefields. Icefield-wide values and associated uncertainties (top right numbers) are given for NPI and SPI both for this study (blue) as well as for the most recent FG estimate[21]. For this study, individual discharge values are given for the most prominent MALT glaciers (numbers ± uncertainties, blue bars). Whiskers indicate associated uncertainties, partitioned into the contribution from the thickness uncertainty (yellow), the velocity error (black) and the integration of the apparent mass balance error (pink). Values from two other recent flux gate (FG) studies[8,21] (green and purple bars) are provided together with independent estimates from mass budgeting (MB) for some individual glaciers[6,8] (red bars). These studies reported on their uncertainties (grey whiskers). For all predecessor studies, some glaciers of SPI (i.e., Bernardo, Témpano, Occidental and Greve) have been aggregated into compounds. For compounds, combined discharge values are represented by bars with dashed outlines and light shading. Note that all estimates have distinct time coverage.

uncertainties reported along geodetic mass changes, it appears that an adequate description of the surface mass balance conditions of the icefields remains, to this day, evasive. This is substantiated by a typical overestimation of precipitation amounts by regional climate models in this area[10]. Moreover, because of the year-round strong westerly winds, snow-drift is a key process in redistributing mass input over the large plateau areas and between the various drainage basins of the icefields. On icefield-wide scales, an appropriate quantification of both precipitation and snow drift continues to be a key challenge in Patagonia.

Data & methods

Reconstruction approaches. For reconstructing 2D maps of basal topography, we rely on a two-step mass-conserving approach[38], which readily assimilates available thickness measurements on regional scales[1,39]. In the first step, we employ two strategies to infer basin-wide thickness fields without using velocity observations. The first strategy is the classical iterative method, which casts the problem with respect to the ice-flux. The flux is subsequently converted into a thickness field by relying on the shallow ice approximation (SIA)[40]. This conversion relies on a spatially variable viscosity field B, which is determined where thickness observations are available. This classical method has further been updated with a viscosity re-scaling that improves the thickness distribution away from observations[60]. The second strategy is a 2D adaptation of a PPA approach[61]. It assumes that the local driving stress τ_d equals a material-specific yield stress τ_0. Similar to above, τ_0 is estimated where thickness measurements are available and subsequently interpolated. To accommodate for non-local stress coupling[62], the driving stress field is spatially smoothed as described in the original first-step approach[38]. This smoothing initially uses a constant radius and is updated once. The thickness field from each strategy independently serves as boundary conditions for the second-step reconstruction, which directly updates the ice thickness in a sub-domain where surface velocities exceed 100 m yr^{-1}. The two thickness maps are then averaged to infer a multi-model estimate. Model parameters are given in Supplementary Table S3. The triangular model mesh has target resolution of 400 m, which is refined near the measurements (~200 m). For the final thickness map, results are interpolated to a 200 m rectangular grid.

Data

Glacier outlines. Two glacier inventories are consulted for outline information. Reference outlines are taken from the Randolph Glacier Inventory version 6.0 (RGI6.0)[3,4]. For this data base, glacier extents have been manually mapped from Landsat images in March 2001[63,64]. This reference extent serve as a basis for the thickness mapping of ice-covered areas. A more recent inventory was required to delineate glacier retreat. It has a 2016 timestamp and was digitised from multiple Landsat scenes[47].

Surface elevation & elevation changes. The reference digital elevation model (DEM) from February 2000 is based on the C-band 30-m product of the Shuttle Radar Topography Mission (SRTM, v2.1)[41]. Remaining voids in steep slope terrain were filled with the 2010 Global multi-resolution terrain elevation data[65]. The SRTM vertical accuracy is smaller than 9m. To determine elevation-change rates after 2000, we rely on the TerraSAR-X-Add-on for DigitalElevation Measurements (TDX)[66]. Elevation change rates have been inferred for both icefields from TDX imagery acquired between 2011 and 2016[17,67]. A second DEM with a more specific time stamp was inferred from TDX coverage in 2019.

Surface mass balance. A combination of dynamical and statistical downscaling techniques were used to infer high-resolution climatic conditions for 1975–2011 from NCEP-NCAR atmospheric reanalysis data[68] over the NPI[6] and the SPI[8]. On this basis, the glacier SMB was estimated using an enhanced temperature index model accounting for cloud-cover corrected potential incoming radiation. From a comparison between geodetic mass changes[17,67] and SMB values over drainge basins of land-terminating glaciers, we infer a specific uncertainty of ~1 myr^{-1} in water equivalent (w.e.). This value comprises both the uncertainty in the elevation change observations as well as in the SMB model estimate. It therefore serves as the input uncertainty for the apparent mass balance.

Thickness observations. Despite the multitude of survey campaigns on the Patagonian Icefields (Supplementary Table S1), no single point measurement of ice thickness is included in the current version 3.1.0 of the global Glacier Thickness Database (GlaThiDa)[22,23]. Here we compile thickness information on 1,475,054 point measurements from two primary sources. The first source comprises direct measurement from ground penetrating radar (GPR), seimsics surveys and a borehole (463,822) as well as gravimetry inferred thickness values (489,194). The second source is indirect thickness values inferred from glacier retreat since February 2001. The retreat area is defined by 2016 outline information with respect to RGI6.0. For retreat on land, we estimate past thickness by DEM differencing against SRTM on 30-m resolution (459,442). For marine retreat, available bathymetric measurements were used and added to the SRTM DEM (62,596). For more details on the considered survey campaigns please refer to the Supplementary Material (Section S1).

Experimental design. The timestamp of the pursued thickness reconstruction is tied to the reference SRTM DEM and thus February 2000. The reason for this is that SRTM serves as the geometric input and is key to determine the retreat thickness information (cf. Supplementary Section S1). Unfortunately, we cannot provide a second thickness map for a more recent period. An option would be the 2011–2015 Copernicus DEM[69]. However, the somewhat contemporaneous national glacier inventories of Argentina[70] and Chile[71] show incomplete coverage. For 2000, we first produce two thickness maps, one building on the SIA and the other on the PPA. Both maps are updated in a second step according to the observed velocity field while thickness observations are assimilated. Gravimetric measurements show a very dense coverage. Where they overlap with other measurements, we often observe an underestimation by gravimetry. We therefore introduce a down-weighting of gravimetric measurements at lower elevation (Supplementary Section S2) in order to give priority to other measurements, where available. In a final step, the SIA and PPA thickness maps are distilled into a multi-model map by simple averaging. We thereby follow the advises from the Ice Thickness Models Intercomparison eXperiment (ITMIX) phases 1 & 2[72,73], that multi-model estimates show improved performance.

Frontal ablation & frontal ice discharge. Flux gates (FG) were placed close to the present ice-fronts of all MALT glaciers, acknowledging the quality of the available velocity field at the glacier surface[11]. The ice flux across these gates is computed as the product of the ice thickness and the surface velocity component perpendicular to these gates. In this way, we assume plug flow and negligible vertical shearing near the ice-fronts. To compute frontal ablation, these flux values are corrected by the integrated apparent mass balance field over the tongue area downstream of the FGs. The apparent mass balance is the difference between the SMB and geodetic elevation changes, with the latter being subtracted. Thereby, we deliberately ignore effects from glacier retreat or basal mass balance. We refer to this flux as the frontal ice discharge. Uncertainties in this quantity are computed by linear error propagation using the error map of our thickness product as well as the largest error of the used multi-sensor surface velocity map, which is reported to be ~52 myr^{-1}[11].

Data availability

The bedrock and ice thickness maps will be distributed together with an uncertainty map via https://doi.org/10.5281/zenodo.10165854. Alongside this article, we provide a glacier-by-glacier list of frontal ice discharge from the flux-gate and the mass-budgeting methods as well as flux-gate characteristics as width, average thickness and average ice speed

(Supplementary Data 1 - 4). These tables are also retrievable from https://zenodo.org/records/10400476. All estimates are provided together with associated uncertainties.

Code availability

Pertinent code for the reconstruction is available from GitHub at https://github.com/FAU-glacier-systems/ElmerIce_Thickness_Reconstruction.

Received: 3 July 2023; Accepted: 20 December 2023;
Published online: 22 March 2024

References

1. Farinotti, D. et al. A consensus estimate for the ice thickness distribution of all glaciers on Earth. *Nat. Geosci.* **12**, 22–28 (2019).
2. Millan, R., Mouginot, J., Rabatel, A. & Morlighem, M. Ice velocity and thickness of the world's glaciers. *Nat. Geosci.* **15**, 124–129 (2022).
3. RGI Consortium (ed.) *Randolph Glacier Inventory ? A Dataset of Global Glacier Outlines: Version 6.0: Technical Report* (Global Land Ice Measurements from Space, Colorado, USA. Digital Media, 2017).
4. Randolph Glacier Inventory - A Dataset of Global Glacier Outlines, Version 6 https://doi.org/10.7265/4m1f-gd79 (2017).
5. Garreaud, R. D. The Andes climate and weather. *Adv. Geosci.* **22**, 3–11 (2009).
6. Schaefer, M., Machguth, H., Falvey, M. & Casassa, G. Modeling past and future surface mass balance of the Northern Patagonia Icefield. *J. Geophys. Res. Earth Surface* **118**, 571–588 (2013).
7. Lenaerts, J. T. M. et al. Extreme precipitation and climate gradients in Patagonia revealed by high-resolution regional atmospheric climate modeling". *J. Clim.* **27**, 4607–4621 (2014).
8. Schaefer, M., Machguth, H., Falvey, M., Casassa, G. & Rignot, E. Quantifying mass balance processes on the Southern Patagonia Icefield. *Cryosphere* **9**, 25–35 (2015).
9. Mernild, S. H., Liston, G. E., Hiemstra, C. & Wilson, R. The Andes Cordillera. Part III: Glacier surface mass balance and contribution to sea level rise (1979-2014). *Int. J. Climatol.* **37**, 3154–3174 (2017).
10. Sauter, T. Revisiting extreme precipitation amounts over southern South America and implications for the Patagonian Icefields. *Hydrol. Earth Syst. Sci.* **24**, 2003–2016 (2020).
11. Mouginot, J. & Rignot, E. Ice motion of the Patagonian Icefields of South America: 1984-2014. *Geophys. Res. Lett.* **42**, 1441–1449 (2015).
12. Rignot, E., Mouginot, J. & Scheuchl, B. Ice flow of the Antarctic Ice Sheet. *Science* **333**, 1427–1430 (2011).
13. Rignot, E. & Mouginot, J. Ice flow in Greenland for the International Polar Year 2008-2009. *Geophys. Res. Lett.* **39**, 7 (2012).
14. Joughin, I., Smith, B., Howat, I., Scambos, T. & Moon, T. Greenland flow variability from ice-sheet-wide velocity mapping. *J. Glaciol.* **56**, 415–430 (2010).
15. Mouginot, J., Rignot, E. & Scheuchl, B. Sustained increase in ice discharge from the Amundsen Sea Embayment, West Antarctica, from 1973 to 2013. *Geophys. Res. Lett.* **41**, 1576–1584 (2014).
16. Gourlet, P., Rignot, E., Rivera, A. & Casassa, G. Ice thickness of the northern half of the patagonia icefields of south america from high-resolution airborne gravity surveys. *Geophys. Res. Lett.* **43**, 241–249 (2016).
17. Braun, M. et al. Constraining glacier elevation and mass changes in South America. *Nat. Clim. Change* **9**, 130–136 (2019).
18. Dussaillant, I. et al. Two decades of glacier mass loss along the andes. *Nat. Geosci.* **12**, 802–808 (2019).
19. Zemp, M. et al. Global glacier mass changes and their contributions to sea-level rise from 1961 to 2016. *Nature* **568**, 382–386 (2019).
20. Hugonnet, R. et al. Accelerated global glacier mass loss in the early twenty-first century. *Nature* **592**, 726–731 (2021).
21. Minowa, M., Schaefer, M., Sugiyama, S., Sakakibara, D. & Skvarca, P. Frontal ablation and mass loss of the Patagonian icefields. *Earth Planet. Sci. Lett.* **561**, 116811 (2021).
22. Welty, E. et al. Worldwide version-controlled database of glacier thickness observations. *Earth Syst. Sci. Data* **12**, 3039–3055 (2020).
23. GlaThiDa Consortium. Glacier Thickness Database 3.1.0. https://doi.org/10.5904/wgms-glathida-2020-10 (2020).
24. Carrivick, J., Davies, B., James, W., Quincey, D. & Glasser, N. Distributed ice thickness and glacier volume in southern South America. *Global Planet. Change* **146**, 122–132 (2016).
25. Millan, R. et al. Ice thickness and bed elevation of the Northern and Southern Patagonian Icefields. *Geophys. Res. Lett.* **46**, 6626–6635 (2019).
26. Gruber, S. & Haeberli, W. Permafrost in steep bedrock slopes and its temperature-related destabilization following climate change. *J. Geophys. Res. Earth Surface* **112**, https://agupubs.onlinelibrary.wiley.com/doi/abs/10.1029/2006JF000547 (2007).
27. Huss, M. & Hock, R. Global-scale hydrological response to future glacier mass loss. *Nat. Clim. Change* **8**, 135–140 (2018).
28. Cauvy-Fraunié, S. & Dangles, O. A global synthesis of biodiversity responses to glacier retreat. *Nat. Ecol. Evol.* **3**, 1675–1685 (2019).
29. Farinotti, D., Round, V., Huss, M., Compagno, L. & Zekollari, H. Large hydropower and water-storage potential in future glacier-free basins. *Nature* **575**, 341–344 (2019).
30. Immerzeel, W. W. et al. Importance and vulnerability of the world?s water towers. *Nature* **577**, 364–369 (2020).
31. Ultee, L., Coats, S. & Mackay, J. Glacial runoff buffers droughts through the 21st century. *Earth Syst. Dyn.* **13**, 935–959 (2022).
32. Zekollari, H., Huss, M., Farinotti, D. & Lhermitte, S. Ice-dynamical glacier evolution modeling - a review. *Rev. Geophys.* **60**, e2021RG000754 (2022).
33. Rounce, D. R. et al. Global glacier change in the 21st century: Every increase in temperature matters. *Science* **379**, 78–83 (2023).
34. Shugar, D. H. et al. Rapid worldwide growth of glacial lakes since 1990. *Nat. Hazards* **10**, 939–945 (2020).
35. Iribarren Anacona, P., Mackintosh, A. & Norton, K. Hazardous processes and events from glacier and permafrost areas: lessons from the Chilean and Argentinean Andes. *Earth Surface Processes Landforms* **40**, 2–21 (2014).
36. Giesecke, R., Höfer, J., Vallejos, T. & González, H. Death in southern Patagonian fjords: Copepod community structure and mortality in land- and marine-terminating glacier-fjord systems. *Progr. Oceanogr.* **174**, 162–172 (2019).
37. Rivera, A., Aravena, J., Urra, A. & Reid, B. Chilean Patagonian glaciers and environmental change. In: *Conservation in Chilean Patagonia: Assessing the state of knowledge, opportunities, and challengers* (Springer Serie Integrated Science, 2021).
38. Fürst, J. et al. Application of a two-step approach for mapping ice thickness to various glacier types on svalbard. *Cryosphere* **11**, 2003–2032 (2017).
39. Fürst, J. et al. The ice-free topography of Svalbard. *Geophys. Res. Lett.* **45**, 11,760–11,769 (2018).
40. Hutter, K. *Theoretical glaciology. Material science of ice and the mechanics of glaciers and ice sheets* (Publishing Company/Tokyo, Terra Scientific Publishing Company, Dordrecht, Boston, Tokyo, Japan, and Hingham, 1983).
41. Farr, T. et al. The shuttle radar topography mission. *Rev. Geophys.* **45**, https://doi.org/10.1029/2005RG000183 (2007).
42. Briner, J., Bini, A. & Anderson, R. Rapid early Holocene retreat of a Laurentide outlet glacier through an Arctic fjord. *Nat. Geosci.* **2**, 496–499 (2009).
43. Rivera, A., Koppes, M., Bravo, C. & Aravena, J. C. Little Ice Age advance and retreat of Glaciar Jorge Montt, Chilean Patagonia. *Clim. Past* **8**, 403–414 (2012).
44. Bown, F. et al. Recent ice dynamics and mass balance of Jorge Montt Glacier, Southern Patagonia Icefield. *J. Glaciol.* **65**, 732–744 (2019).
45. Koppes, M., Hallet, B. & Anderson, J. Synchronous acceleration of ice loss and glacial erosion, Glaciar Marinelli, Chilean Tierra del Fuego. *J. Glaciol.* **55**, 207–220 (2009).
46. Davies, B. & Glasser, N. Accelerating shrinkage of Patagonian glaciers from the Little Ice Age (AD 1870) to 2011. *J. Glaciol.* **58**, 1063–1084 (2012).
47. Meier, W., Grießinger, J., Hochreuther, P. & Braun, M. An Updated Multi-Temporal Glacier Inventory for the Patagonian Andes With Changes Between the Little Ice Age and 2016. *Front. Earth Sci.* **6**, 1–21 (2018).
48. Rivera, A. et al. Estudio de la profundidad del lago Viedma, Parque Nacional Los Glaciares, Argentina. *GEOACTA* **42**, 4–6 (2018).
49. Hauthal, R.*Gletscherbilder aus der argentinischen Cordillere*, vol. 35 (Zeitschrift des Deutschen und Österreichischen Alpenvereins, 1904).
50. Lodolo, E. et al. The submerged footprint of Perito Moreno Glacier. *Sci. Rep.* **10**, 16437 (2020).
51. Sugiyama, S. et al. Thermal structure of proglacial lakes in Patagonia. *J. Geophys. Res. Earth Surface* **121**, 2270–2286 (2016).
52. Sugiyama, S. et al. Subglacial discharge controls seasonal variations in the thermal structure of a glacial lake in Patagonia. *Nat. Commun.* **12**, 6301 (2021).
53. Minowa M, Schaefer M, Skvarca P. Effects of topography on dynamics and mass loss of lake-terminating glaciers in southern Patagonia. *J. Glaciol.* 1–18 https://doi.org/10.1017/jog.2023.42 (2023).
54. Weidemann, S. et al. Glacier mass changes of lake-terminating Grey and Tyndall glaciers at the Southern Patagonia Icefield derived from geodetic observations and energy and mass balance modeling. *Front. Earth Sci.* **6**, 81 (2018).
55. Temme, F. et al. Strategies for regional modeling of surface mass balance at the monte sarmiento massif, tierra del fuego. *Cryosphere* **17**, 2343–2365 (2023).
56. Zekollari, H. & Huybrechts, P. On the climate-geometry imbalance, response time and volume?area scaling of an alpine glacier: insights from a 3-D flow model applied to Vadret da Morteratsch, Switzerland. *Ann. Glaciol.* **56**, 51–62 (2015).

57. Huss, M. & Farinotti, D. Distributed ice thickness and volume of all glaciers around the globe. *J. Geophys. Res.* **117**, 10 (2012).
58. Maussion, F. et al. The Open Global Glacier Model (OGGM) v1.1. *Geosci. Model Dev.* **12**, 909–931 (2019).
59. Schwikowski, M., Schläppi, M., Santibañez, P., Rivera, A. & Casassa, G. Net accumulation rates derived from ice core stable isotope records of Pío XI glacier, Southern Patagonia Icefield. *Cryosphere* **7**, 1635–1644 (2013).
60. Sommer, C., Fürst, J., Huss, M. & Braun, M. Constraining regional ice thickness with glacier retreat observations in the European Alps. *Cryosphere* **17**, 2285–2303 (2022).
61. Linsbauer, A., Paul, F. & Haeberli, W. Modeling glacier thickness distribution and bed topography over entire mountain ranges with GlabTop: Application of a fast and robust approach. *J. Geophys. Res.* **117**, n/a–n/a (2012).
62. Hindmarsh, R. The role of membrane-like stresses in determining the stability and sensitivity of the Antarctic ice sheets: back pressure and grounding line motion. *Philos. Trans. R. Soc. A* **364**, 1733–1767 (2006).
63. Rivera, A., Benham, T., Casassa, G., Bamber, J. & Dowdeswell, J. Ice elevation and areal changes of glaciers from the Northern Patagonia Icefield, Chile. *Global Planet. Change* **59**, 126–137 (2007).
64. De Angelis, H. Hypsometry and sensitivity of the mass balance to changes in equilibrium-line altitude: the case of the Southern Patagonia Icefield. *J. Glaciol.* **60**, 14–28 (2014).
65. Danielson, J. & Gesch, D. *Global multi-resolution terrain elevation data 2010 (GMTED2010)*, 2011-1073. USGS Earth Resources Observation and Science (EROS) Center, 2011).
66. Krieger, G. et al. TanDEM-X: A radar interferometer with two formation-flying satellites. *Acta Astronautica* **89**, 83–89 (2013).
67. Malz, P. et al. Elevation and mass changes of the Southern Patagonia icefield derived from TanDEM-X and SRTM data. *Remote Sensing* **10**, 188 (2018).
68. Kalnay, E. et al. The NCEP/NCAR 40-year reanalysis project. *Bull. Am. Meteorol. Soc.* **77**, 437–472 (1996).
69. EU & ESA. Copernicus DEM - Global and European Digital Elevation Model (COP-DEM) (DLR e.V. 2010-2014 and Airbus Defence and Space GmbH 2014-2018 provided under COPERNICUS by the European Union (EU) and the European Space Agency (ESA). https://spacedata.copernicus.eu/collections/copernicus-digital-elevation-model (2019).
70. IANIGLA & CONICET. Inventario Nacional de Glaciares (ING). IF-2018-23356401-APN-DNGAAYEA#MAD (Ministerio de Ambiente y Desarrollo Sustentable - Presidencia de la Nación, Instituto Argentino de Nivología, Glaciología y Ciencias Ambientales (IANIGLA) & Consejo Nacional de Investigaciones Científicas y Técnicas (CONICET). https://www.glaciaresargentinos.gob.ar/wp-content/uploads/resultados_finales/informe_resumen_ejecutivo_APN_11-05-2018.pdf (2018).
71. DGA. Inventario Público de Glaciares 2014 (Ministerio de Obras Públicas, Dirección General de Aguas (DGA), Unidad de Glaciología y Nieves, 2014). https://snia.mop.gob.cl/repositoriodga/handle/20.500.13000/125854.
72. Farinotti, D. et al. How accurate are estimates of glacier ice thickness? Results from ITMIX, the Ice Thickness Models Intercomparison eXperiment. *Cryosphere* **11**, 949–970 (2017).
73. Farinotti, D. et al. Results from the Ice Thickness Models Intercomparison eXperiment Phase 2 (ITMIX2). *Front. Earth Sci.* **8**, 571923 (2021).
74. Liboutry, L.*Nieves y glaciares de Chile. Fundamentos de Glaciología* (Universidad de Chile, 1956).
75. Mercer, J. *Southern Hemisphers glacier atlas [in Technical Report W-67-76-ES.]* (Earth Science Laboratory, Natick Laboratories, United States Army, Natick, MA, USA, 1967).

Acknowledgements
The main author J.J.F. received primary funding from the European Union's Horizon 2020 research and innovation programme via the European Research Council (ERC) as a Starting Grant (FRAGILE project) under grant agreement No 948290. D.F.-B. was funded by the German Research Foundation (DFG) within the MAGIC and ITERATE projects (FU1032/5-1, BR2105/28-1, FU1032/12-1) as well as the ANID Subvención a la instalación a la academia 2022 (PAI85220007), Fondecyt N°3230146, and Anillo ACT210080. F.G.-C. was funded by the ANR MAGIC project, grant ANR-19-CE01-0023 of the French Agence Nationale de la Recherche. M.P. received support from ANID INICIACIÓN 11170937 grant and from the Priority Research Area (Anthropocene) under the Strategic Programme Excellence Initiative at Jagiellonian University. The 'Alexander von Humboldt Foundation' provided support to M.S. (grant ID: Ref 3.2 - 1216763 - CHL - HFST-E). We further want to acknowledge the candid support we received from Chilean colleagues at the 'Unidad de Glaciología y Nieves' of the 'Dirección General de Aguas' (DGA) within the 'Ministerio de Obras Públicas' and at the 'Centro de Estudios Científicos' (CECs) in Valdivia, Chile as well as at the 'Servicio Hidrográfico y Oceanográfico de la Armada de Chile' (SHOA). Also on the Argentinian side, important support was received from colleagues at the University of Buenos Aires for bathymetric surveys in the lateral branches of Lago Argentino. Moreover, we greatly acknowledge the courtesy of the Geographical Military Institute (IGM) of Chile to make available aerial photographs for this publication, including acquisitions from the US Air Force. Further appreciation is at order for radar data acquired with the Warm Ice Sounding Explorer (WISE) operated and maintained by the National Aeronautics and Space Administration (NASA). For elevation change products, the authors would like to thank the German Aerospace Centre for providing TanDEM-X data free of charge under AO XTI_GLAC0264. Moreover, we want to express our recognition for the long-term efforts to consolidate global glacier outline information in the Randolph Glacier Inventory (Technical Report). Finally, the authors gratefully acknowledge the scientific support and HPC resources provided by the Erlangen National High Performance Computing Centre (NHR@FAU) of the Friedrich-Alexander-Universität Erlangen-Nürnberg (FAU). NHR funding is provided by federal and Bavarian state authorities. NHR@FAU hardware is partially funded by the German Research Foundation (DFG) - 440719683. The reconstruction approach also benefits from continuous co-development work of the Elmer/Ice team at the CSC-IT Centre for Science Ltd (Finland).

Author contributions
G.C. initiated the application of the reconstruction approach to the Patagonian icefields. J.J.F. designed the study, implemented the perfect-plasticity reconstruction variant and led the analysis. For data acquisition, J.J.F. was strongly supported by D.F.-B. The research setup and targeted objectives were developed in regular discussions with D.F.-B. Objectives were further revised with valuable input from P.S. and M.S. N.B., G.C., G.G., M.K., E.L., R.M., M.M., M.P., E.R., A.R., M.S., S.S., J.U. and R.Z. revised and provided their point measurements on ice thickness or lake/fjord bathymetries. Elevation changes and DEMs were generated and provided by D.F.-B., M.H.B and P.M. Surface mass balances and 2016 glacier outlines were shared by M.S. and W.J.-H.M, respectively. The 2004 surface velocity mosaic was key and made available by J.M. Software maintenance and technical support from F.G.-C. was essential to render the conducted experiments possible. All authors contributed to the interpretation of the results and to the writing of the manuscript, both under the coordination of J.J.F.

Funding
Open Access funding enabled and organized by Projekt DEAL.

Competing interests
S.S. is an Editorial Board Member for Communications Earth & Environment, but was not involved in the editorial review of, nor the decision to publish this article. The other authors declare no competing interests.

Additional information
Supplementary information The online version contains supplementary material available at https://doi.org/10.1038/s43247-023-01193-7.

Correspondence and requests for materials should be addressed to Johannes J. Fürst.

Peer review information *Communications Earth & Environment* thanks Kátia Kellem da Rosa, Harold Lovell and William James for their contribution to the peer review of this work. Primary Handling Editors: Joe Aslin. A peer review file is available.